

# $H_0$ Revisited

George Efstathiou

*Kavli Institute for Cosmology and Institute of Astronomy, Madingley Road, Cambridge, CB3 0HA.*

24 May 2022

## ABSTRACT

I reanalyse the Riess *et al.* (2011, hereafter R11) Cepheid data using the revised geometric maser distance to NGC 4258 of Humphreys *et al.* (2013, hereafter H13). I explore different outlier rejection criteria designed to give a reduced  $\chi^2$  of unity and compare the results with the R11 rejection algorithm, which produces a reduced  $\chi^2$  that is substantially less than unity and, in some cases, leads to underestimates of the errors on parameters. I show that there are sub-luminous low metallicity Cepheids in the R11 sample that skew the global fits of the period-luminosity relation. This has a small but non-negligible impact on the global fits using NGC 4258 as a distance scale anchor, but adds a poorly constrained source of systematic error when using the Large Magellanic Cloud (LMC) as an anchor. I also show that the small Milky Way (MW) Cepheid sample with accurate parallax measurements leads to a distance to NGC 4258 that is in tension with the maser distance. I conclude that  $H_0$  based on the NGC 4258 maser distance is  $H_0 = 70.6 \pm 3.3 \text{ km s}^{-1} \text{ Mpc}^{-1}$ , compatible within  $1\sigma$  with the recent determination from *Planck* for the base six-parameter  $\Lambda$ CDM cosmology. If the H-band period-luminosity relation is assumed to be independent of metallicity and the three distance anchors are combined, I find  $H_0 = 72.5 \pm 2.5 \text{ km s}^{-1} \text{ Mpc}^{-1}$ , which differs by  $1.9\sigma$  from the *Planck* value. The differences between the *Planck* results and these estimates of  $H_0$  are not large enough to provide compelling evidence for new physics at this stage.

**Key words:** cosmology: distance scale, cosmological parameters.

## 1 INTRODUCTION

The recent *Planck* observations of the cosmic microwave background (CMB) lead to a Hubble constant of  $H_0 = 67.3 \pm 1.2 \text{ km s}^{-1} \text{ Mpc}^{-1}$  for the base six-parameter  $\Lambda$ CDM model (Planck Collaboration 2013, hereafter P13). This value is in tension, at about the  $2.5\sigma$  level, with the direct measurement of  $H_0 = 73.8 \pm 2.4 \text{ km s}^{-1} \text{ Mpc}^{-1}$  reported by R11. If these numbers are taken at face value, they suggest evidence for new physics at about the  $2.5\sigma$  level (for example, exotic physics in the neutrino or dark energy sectors as discussed in P13; see also Wyman *et al.* 2013, Hamann and Hasenkamp 2013; Battye and Moss 2013; Rest *et al.* 2013; Suyu *et al.* 2013). The exciting possibility of discovering new physics provides strong motivation to subject both the CMB and  $H_0$  measurements to intense scrutiny.

Direct astrophysical measurements of the Hubble constant have a checkered history (see, for example, the reviews by Tammann, Sandage and Reindl 2008; Freedman and Madore 2010). The Hubble Space Telescope (HST) Key Project led to a significant improvement in the control of systematic errors leading to ‘final’ estimate of  $H_0 = 72 \pm 8 \text{ km s}^{-1} \text{ Mpc}^{-1}$  (Freedman *et al.* 2001). Since then, two Cepheid based programmes have been underway with the aim of reducing the error on  $H_0$ : the *Supernovae and  $H_0$  for the Equation of State* (SH0ES) programme of R11 (with earlier results reported in Riess *et al.* 2009) and the *Carnegie Hubble Program* of Freedman *et al.* (2012). In addition, other programmes are underway using geometrical methods, for example the Megamaser Cosmology Project (MCP) (Reid *et al.* 2013; Braatz *et al.* 2013) and the Cosmological Monitoring of Gravitational Lenses (COSMOGRAIL) project (Suyu *et al.* 2010, Courbin *et al.* 2011; Treves *et al.* 2013).

This paper presents a reanalysis of the R11 Cepheid data. The  $H_0$  measurement from these data has the smallest error and has been used widely in combination with CMB measurements for cosmological parameter analysis (*e.g.* Hinshaw *et al.* 2012; Hou *et al.* 2012; Sievers *et al.* 2013). The study reported here was motivated by certain aspects of the R11 analysis: the R11 outlier rejection algorithm (which rejects a large fraction,  $\sim 20\%$ , of the Cepheids), the low reduced  $\chi^2$  values of their fits,

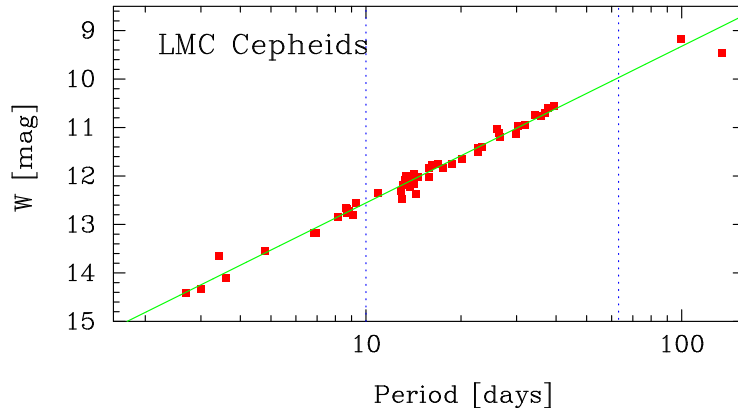


**Figure 1.** Period-luminosity relation for the LMC Cepheids. The line shows the best fit of equation (4a). The vertical dotted lines show the range of periods used in the fit of equation (4b).

and the variations of some of the parameter values with different distance anchors, particularly the metallicity dependence of the period-luminosity relation.

The layout of this paper is as follows. Section 2 reviews the near-IR period-luminosity (P-L) relation of a sample of LMC Cepheids. Section 3 describes a reanalysis of the R11 sample using the maser distance to NGC 4258 as an anchor. Section 4 investigates the use of the LMC and MW Cepheids as anchors. Section 5 investigates combinations of the three distance anchors and presents some internal consistency checks. The conclusions are summarized in Section 6.

## 2 THE LMC CEPHEIDS

I will start with the LMC Cepheids which I will use as a reference since the slope of the P-L relation is tightly constrained from this sample. I use the 53 LMC Cepheids with H-band magnitudes listed in Persson *et al.* (2004) and V, I magnitudes listed in Sebo *et al.* (2002). Figure 1 shows the Wesenheit magnitudes

$$m_W = m_H - 0.41(V - I), \quad (1)$$

plotted against period  $P$  (in units of days). The line shows a least-squares fit to

$$m_W^P = A + b_W (\log P - 1), \quad (2)$$

*i.e.* minimising

$$\chi^2 = \sum_i \frac{(m_{W,i} - m_W^P)^2}{(\sigma_{e,i}^2 + \sigma_{\text{int}}^2)}, \quad (3)$$

where  $\sigma_{e,i}$  is the error on  $m_{W,i}$  and  $\sigma_{\text{int}}$  is the ‘internal’ scatter that gives a reduced  $\chi^2$  (denoted  $\hat{\chi}^2$  in this paper) of unity. Since  $\sigma_{\text{int}}$  depends on the parameters  $A$  and  $b_W$ , the minimisation is performed iteratively until convergence. The best fit parameters are

$$A = 12.555 \pm 0.018, \quad b_W = -3.23 \pm 0.06, \quad \sigma_{\text{int}} = 0.113, \quad \log P < 1.8, \quad (4a)$$

$$A = 12.594 \pm 0.034, \quad b_W = -3.35 \pm 0.11, \quad \sigma_{\text{int}} = 0.104, \quad 1.0 < \log P < 1.8. \quad (4b)$$

The upper period limit is imposed because there is evidence that the P-L relation departs from a power law for periods  $\gtrsim 60$  days (Persson *et al.*, 2004; Freedman *et al.* 2011; Scowcroft *et al.* 2011). The lower period limit in (4b) has been imposed because there have been some claims that the P-L relation at optical and near-IR wavelengths changes at periods less than 10 days (Ngeow *et al.* 2009). The results of (4a) and (4b) and Figure 1 show no evidence for any significant change in the power-law slope at low periods, in agreement with the results of Persson *et al.* (2004). Evidently, a single power law is an extremely good fit to the LMC Cepheids at least to periods of 60 days, and the slope of the P-L relation is determined to high accuracy.

Galaxy	$N_{\text{fit}}$	$N_{\text{rej}}$	H mags		W mags	
			$\sigma$ (mag)	$\hat{\chi}^2$	$\sigma$ (mag)	$\hat{\chi}^2$
N4536	69	20	0.32	1.25	0.33	1.22
N4639	32	6	0.41	1.25	0.41	1.24
N3370	79	10	0.32	0.90	0.32	0.89
N3982	29	22	0.32	0.79	0.33	0.84
N3021	26	4	0.39	0.73	0.39	0.74
N1309	36	4	0.31	0.95	0.32	0.98
N5584	95	17	0.32	1.01	0.32	1.04
N4038	39	7	0.34	0.77	0.36	0.97
N4258	164	46	0.36	1.01	0.37	0.98

**Table 1.** H-band rejection.  $N_{\text{fit}}$  and  $N_{\text{rej}}$  lists the number of Cepheids accepted and rejected by the R11 outlier rejection algorithm.  $\sigma$  is the standard deviation of the magnitude residuals about the best fit P-L relation with slope constrained to  $b = -3.1$  and  $\hat{\chi}^2$  lists the reduced  $\chi^2$  for each fit (with no additional contribution from ‘intrinsic’ scatter). Results are given for fits to H-band and Wesenheit P-L relations.

### 3 ANALYSIS OF THE R11 CEPHEID SAMPLE USING NGC 4258 AS AN ANCHOR DISTANCE

#### 3.1 Outlier rejection

As discussed by R11, there are several reasons to expect outliers in the P-L relation. These include variables misidentified as classical Cepheids, blended images, errors in crowding corrections and possible aliasing of the periods.

The R11 rejection algorithm works as follows:

- The H-band only P-L relations are fitted galaxy-by-galaxy to a power law with slope fixed at  $b_H = -3.1$  in the first iteration, weighted by the magnitude errors in Table 2 of R11. Cepheids with periods  $> 205$  days are excluded.
- Cepheids are rejected if they deviate from the best-fit relation by  $\geq 0.75$  mag, or by more than 2.5 times the magnitude error.
- The fitting and rejection is repeated iteratively 6 times.

Once the outliers have been removed, R11 proceed to global fits using all of their galaxies, now adding a 0.21 mag. error in quadrature to the magnitude errors listed in their Table 2 (Riess, private communication). One of the consequences of adding this additional error term is that the  $\hat{\chi}^2$  values of the R11 global fits are always less than unity (with typical values of  $\hat{\chi}^2 \sim 0.65$ ) so R11 rescale their covariance matrices by  $1/\hat{\chi}^2$  to compute errors on parameters.

There are several aspects about this rejection algorithm that are worrisome:

- The rejection algorithm is applied galaxy-by-galaxy *before* the global fit to the entire sample.
- A large fraction of the data are rejected (about 20% of the total sample).
- The imposition of an absolute cut of 0.75 mag will accept points with large magnitude errors and small residuals, *i.e.* points that just happen to lie close to the best-fit P-L relation for each galaxy.
- As a consequence,  $\hat{\chi}^2$  for the *global fits* is guaranteed to be less than unity if an additional ‘intrinsic’ error of 0.21 mag is added to the magnitude errors.

The last three points are evident from the entries in Table 1.  $N_{\text{fit}}$  is the number of Cepheids accepted by R11 and  $N_{\text{rej}}$  is the number rejected.  $\sigma$  is the standard deviation of the magnitude residuals of the accepted Cepheids around the best fit P-L relation with slope constrained to  $b = -3.1$ .  $\hat{\chi}^2$  gives the reduced  $\chi^2$  computed using the magnitude errors listed in R11. Although the dispersions exceed 0.3 mag., the values of  $\hat{\chi}^2$  for many galaxies are already less than unity. I also list results for fits to the Wesenheit magnitudes (1). These numbers are similar to those for the H-band fits, so adding colour information produces very little change to the scatter. Since the values of  $\hat{\chi}^2$  in Table 1 are already low,  $\hat{\chi}^2$  for the global fits will be substantially less than unity if an additional 0.21 mag. is added in quadrature to the R11 magnitude errors. Table 1 shows that there is simply no room for additional scatter (irrespective of colour corrections). The choice of adding a 0.21 magnitude error to the Cepheids accepted by the R11 rejection algorithm is not supported by the data.

Instead of rejecting Cepheids on a galaxy-by-galaxy basis, I reject outliers from the global fit. As in R11, we write the P-L relation for galaxy  $i$  as

$$m_{W,i}^P = (\mu_{0,i} - \mu_{0,4258}) + p_W + Z_W \Delta \log(\text{O/H}) + b_W \log P, \tag{5}$$

and minimise,

$$\chi_{\text{WFC3}}^2 = \sum_{ij} \frac{(m_{W,ij} - m_{W,i}^P)^2}{(\sigma_{e,ij}^2 + \sigma_{\text{int}}^2)}, \tag{6}$$

(where  $j$  is the index of the Cepheid belonging to galaxy  $i$  and  $\sigma_{e,ij}$  is the magnitude error listed in Table 2 of R11) with

Global fits: NGC 4258 anchor

Fit	$N_{\text{fit}}$	$\hat{\chi}_{\text{WFC3}}^2$	$H_0$	T=2.5 Rejection			$Z_w$	$\sigma_{\text{int}}$	Priors	
				$p_W$	$b_W$				$Z_w$	$b_W$
1	485	1.00	71.1 (3.2) (2.4)	26.30 (0.17)	-3.05 (0.13)	-0.45 (0.15)	0.32	N	N	
2	484	1.00	70.3 (3.2) (2.4)	26.35 (0.17)	-3.08 (0.13)	-0.31 (0.13)	0.32	W	N	
3	481	1.00	69.7 (3.1) (2.3)	26.38 (0.16)	-3.10 (0.12)	-0.006 (0.020)	0.32	S	N	
4	482	1.00	69.0 (3.0) (2.1)	26.49 (0.11)	-3.18 (0.08)	-0.006 (0.020)	0.32	S	Y	
Fit	$N_{\text{fit}}$	$\hat{\chi}_{\text{WFC3}}^2$	$H_0$	T=2.25 Rejection			$Z_w$	$\sigma_{\text{int}}$	Priors	
				$p_W$	$b_W$				$Z_w$	$b_W$
5	458	1.00	70.6 (3.0) (2.1)	26.59 (0.15)	-3.24 (0.11)	-0.53 (0.13)	0.21	N	N	
6	459	1.00	70.3 (3.0) (2.1)	26.59 (0.15)	-3.23 (0.11)	-0.40 (0.11)	0.22	W	N	
7	447	1.00	70.8 (3.0) (2.0)	26.61 (0.14)	-3.22 (0.10)	-0.007 (0.020)	0.18	S	N	
8	447	1.00	70.8 (2.9) (2.0)	26.61 (0.10)	-3.23 (0.07)	-0.007 (0.020)	0.18	S	Y	
Fit	$N_{\text{fit}}$	$\hat{\chi}_{\text{WFC3}}^2$	$H_0$	R11 Rejection			$Z_w$	$\sigma_{\text{int}}$	Priors	
				$p_W$	$b_W$				$Z_w$	$b_W$
9	390	0.64	72.3 (2.8) (1.8)	26.43 (0.13)	-3.10 (0.09)	-0.33 (0.11)	0.21	N	N	
10	390	0.64	72.1 (2.8) (1.8)	26.44 (0.13)	-3.11 (0.10)	-0.25 (0.10)	0.21	W	N	
11	390	0.65	71.2 (2.8) (1.8)	26.48 (0.13)	-3.14 (0.09)	-0.007 (0.016)	0.21	S	N	
12	390	0.65	70.8 (2.7) (1.7)	26.56 (0.09)	-3.19 (0.06)	-0.007 (0.016)	0.21	S	Y	

**Table 2.**  $N_{\text{fit}}$  gives the number of Cepheids accepted by the outlier rejection criteria. The numbers in brackets give the  $1\sigma$  errors on the parameters computed from the diagonals of the inverse covariance matrix. For  $H_0$  the first number in brackets gives the total error on the Hubble constant, including the megamaser distance error and the SNe magnitude errors. The second number in brackets lists the error in  $H_0$  from the P-L relation only. The column labelled  $\sigma_{\text{int}}$  lists the internal scatter. The last two columns indicate the prior applied to metallicity dependence  $Z_W$  (N: no prior; W: weak prior; S: strong prior) and to the P-L slope  $b_W$  (N: no prior; Y: prior) as summarized in (8a) - (8c). Fits 1-4 list results for  $T = 2.5$  outlier rejection, fits 5-8 for  $T = 2.25$  outlier rejection and fits 9-12 for the R11 rejection algorithm.

respect to the parameters of the global fit. I use only Cepheids with periods  $P < 60$  days in these fits. (See the Appendix A for remarks on the effects of extending the period range).

I set  $\sigma_{\text{int}} = 0.30$  initially and reject Cepheids with absolute magnitude residuals relative to the global fit that are greater than  $T\sqrt{(\sigma_{e,ij}^2 + \sigma_{\text{int}}^2)}$  for a chosen threshold  $T$ . I then recompute  $\sigma_{\text{int}}^2$  to give  $\hat{\chi}^2 = 1$  and repeat until the fits and rejection conditions converge. The algorithm is statistically self consistent<sup>1</sup>, in the sense that the solutions converge with  $\hat{\chi}^2 = 1$  for a positive value of  $\sigma_{\text{int}}^2$ , as long as  $T$  is chosen to be greater than  $T = 2.1$ . Below I will show results for  $T = 2.5$  and  $T = 2.25$ . Both this and the R11 rejection algorithm are symmetrical about the best fits and could introduce biases if the residuals are distributed asymmetrically. Unfortunately, the Cepheid sample is not large enough to apply statistically meaningful tests for asymmetric residuals.

The term  $\sigma_{\text{int}}$  is expected to be non-zero since there will be scatter in the P-L relation from the finite width of the instability strip. The analysis of the LMC Cepheids in Section 2 suggests that at H-band the internal scatter of the P-L relation is about 0.1 mag (though the geometrical distribution of the LMC Cepheids contributes to some of this scatter). R11 make no phase corrections to the H-band magnitudes and estimate that this introduces an additional scatter of about 0.1 mag. Combining these contributions suggests a minimum value of  $\sigma_{\text{int}} \approx 0.14$  mag. Systematic under-estimation of magnitude errors (*e.g.* crowding corrections) or contamination by outliers will result in higher values of  $\sigma_{\text{int}}$ .

Results of the global fits, propagated through to values of  $H_0$ , are listed in Table 2. Here I have used the new NGC 4258 maser distance of  $7.60 \pm 0.23$  Mpc (H13) which improves on the maser distance of Herrnstein *et al.* (1999) and is higher than the distance adopted by R11 of  $7.28 \pm 0.22$  Mpc (see Riess *et al.*, 2012). This change alone revises  $H_0$  downwards by approximately  $3 \text{ km s}^{-1} \text{ Mpc}^{-1}$ . The SNe magnitudes and errors as listed in Table 3 of R11. Figure 2 shows the magnitude residuals with respect to global fit number 5 for Cepheids in NGC 4258 (left) and for the SNe host galaxies (right). The results of Table 2 are in agreement with the conclusion of R11, namely that the primary sensitivity to outliers comes from a small number of highly deviant points that are easy to identify and that are rejected by all three rejection conditions. However, the effects of applying different rejection criteria is non-negligible. Comparing pairs of fits with the different outlier rejection conditions explored in in Table 2 shows differences in  $H_0$  of  $\sim 1.5 \text{ km s}^{-1} \text{ Mpc}^{-1}$ . An estimate of the error associated with outlier rejection should therefore be folded into the total error on  $H_0$ . (In fact, R11 add  $0.8 \text{ km s}^{-1}$  in quadrature to their final error estimate on  $H_0$  to account for systematic errors such as sensitivity to outlier rejection.)

<sup>1</sup> For a Gaussian distribution, the application of a threshold rejection will bias  $\hat{\chi}^2$  low by factors of 0.921 and 0.856 for  $T = 2.5$  and  $T = 2.25$  respectively. These biases are neglected in this analysis.

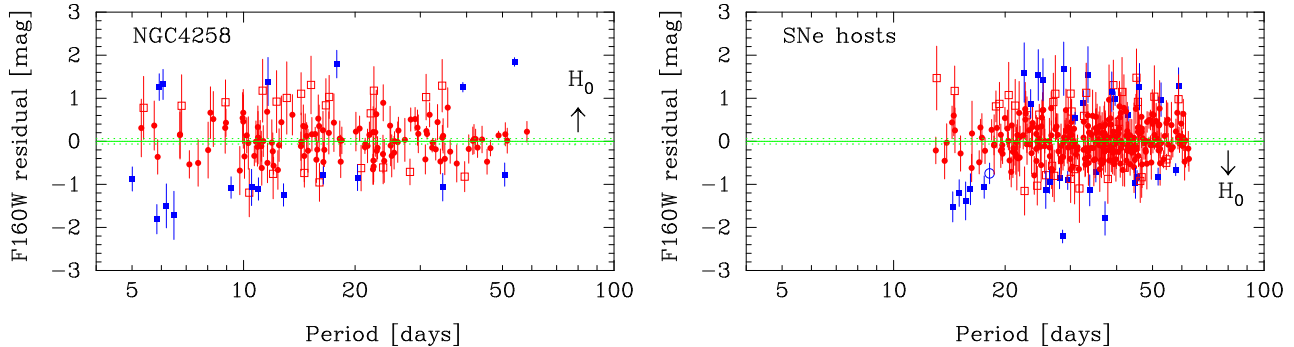


**Figure 2.** P-L magnitude residuals relative to global fit 5 of Table 2: Residuals for NCG4258 Cepheids are shown on the left and the SNe host galaxy Cepheids are shown on the right. Filled (red) dots show residuals for Cepheids that are accepted by both the R11 and the  $T = 2.25$  rejection criterion. Filled (blue) squares are rejected by both algorithms. Open (red) squares are rejected by R11 but accepted by the  $T = 2.25$  rejection criterion and the single open (blue) circle is rejected by the  $T = 2.25$  criterion but accepted by R11. The errors show the H-band magnitude errors as listed in R11. The dotted lines show offsets that would produce changes of  $\pm 2 \text{ km s}^{-1} \text{ Mpc}^{-1}$  in the value of  $H_0$  (increasing  $H_0$  is shown by the direction of the arrow in each plot).

### 3.2 Metallicity dependence

More worryingly, fits 1, 5 and 9 all show a strong metallicity dependence, apparently at the  $3 - 4\sigma$  significance level. The metallicity dependence of the P-L relation has been controversial for many years. At optical wavelengths, there is evidence for a metallicity dependence of  $\sim -0.25 \text{ mag. dex}^{-1}$  (Kennicutt *et al.* 1998; Sakai *et al.* 2004, Macri *et al.* 2006; Scowcroft *et al.* 2009). There are also theoretical arguments (McGonegal *et al.* 1982) and some empirical constraints (Freedman and Madore 2011; Scowcroft *et al.* 2013) to suggest that the metallicity dependence of the P-L relation at near-IR and mid-IR wavelengths should be weaker than at optical wavelengths. In fact, in a recent study of the P-L relation for LMC Cepheids with spectroscopic  $[\text{Fe}/\text{H}]$  measurements, Freedman and Madore (2011) find

$$Z_H = 0.05 \pm 0.02 \text{ mag. dex}^{-1}, \tag{7}$$

for the metallicity dependence at H-band. An updated version of this analysis is presented in Freedman *et al.* (2011) in which the metallicity dependence of LMC Cepheids at H-band appears to be even weaker than in equation (7). Equation (7) clearly conflicts with the results of Table 2<sup>2</sup>.

Yet as can be seen from Figure 3, the R11 data contain sub-luminous low metallicity Cepheids. In these plots, we show the magnitude residual with respect to fit 5, but setting  $Z_w = 0$  (*i.e.* neglecting the metallicity dependence of the P-L relation). The right hand panel of Figure 3 shows low metallicity Cepheids, almost all of which lie below the mean relation. Some of these Cepheids are rejected by R11 but accepted by the  $T = 2.25$  rejection (open red symbols). This is mainly because these Cepheids fail the R11 0.75 mag. cut which is applied to the H-band magnitudes *before* fitting for a metallicity dependence of the P-L relation. This difference in rejection explains why the metallicity dependence is stronger in the  $T = 2.5$  and  $T = 2.25$  fits compared to the R11 fits. However, the metallicity dependence is strong even with the R11 rejection algorithm. It is also worth noting that the metallicity trend extends to Cepheids with  $12 + \log(\text{O}/\text{H}) > 8.6$ . Eliminating the small number of stars with  $12 + \log(\text{O}/\text{H}) < 8.6$  reduces, but does not eliminate, the metallicity dependence of the global fits.

The strong metallicity dependence in the R11 sample may indicate an unidentified systematic in the data. For example, the low metallicity systems may be blended Type II Cepheids that are not identified by the outlier rejection algorithm. Another possibility might be errors in the crowding bias corrections (since the low metallicity Cepheids have lower than average crowding bias corrections). The effect is so large that it seems unlikely that the discrepancy between (7) and the R11 data is related to the use of nebular  $[\text{O}/\text{H}]$  estimates of metallicity rather than spectroscopic  $[\text{Fe}/\text{H}]$  metallicities of individual Cepheids. Additional constraints on  $Z_W$ , based on  $[\text{O}/\text{H}]$  metallicities, are discussed in Section 5.

Another way of reducing the sensitivity to outliers and possible systematics in the data is to impose priors on the parameters of the P-L relation. I have explored the following priors:

$$\langle Z_w \rangle = 0, \quad \sigma_{Z_w} = 0.25, \quad \text{weak metallicity prior}, \tag{8a}$$

<sup>2</sup> The constraint of equation (7) is derived from a small sample of 21 LMC Cepheids. Since the metallicity dependence is a small effect, it is possible that subtle effects such as a correlation between effective temperature and metallicity, or between metallicity and age lead to biases in the inferred metallicity dependence of the P-L relation. Equation (7) is consistent with a weak metallicity dependence of the P-L relation at near-infrared wavelengths, however, both the variation of the metallicity dependence with waveband reported by Freedman and Madore (2011; see also Romaniello *et al.*, 2008) and their error estimates should be treated with caution.

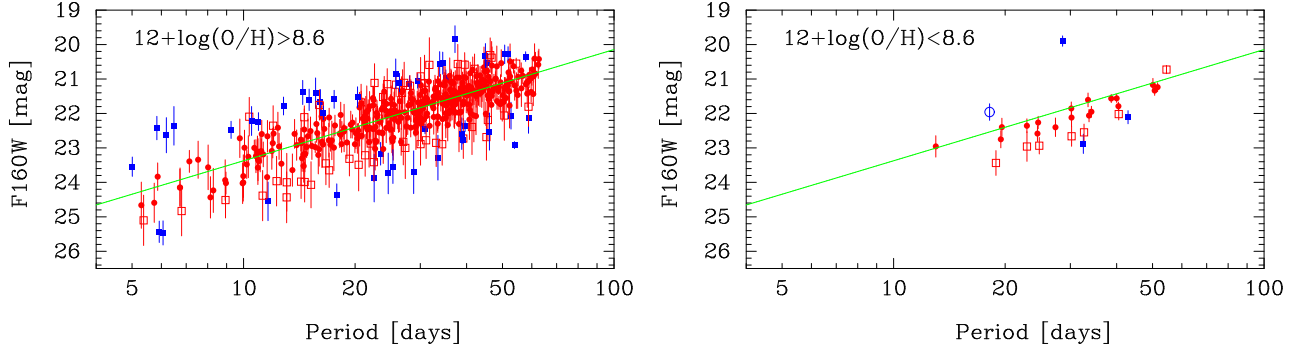


**Figure 3.** P-L relations for the data used in fit 5. The symbols and colour coding of the points are as in Figure 3. In these plots, the F160W magnitudes have not been corrected for a metallicity dependence. The figure to the left shows high metallicity Cepheids and the figure to the right shows low metallicity Cepheids. The lines show the best fit P-L relation for the entire sample.

$$\langle Z_w \rangle = 0, \quad \sigma_{Z_w} = 0.02, \quad \text{strong metallicity prior,} \quad (8b)$$

$$\langle b \rangle = -3.23, \quad \sigma_b = 0.10, \quad \text{P - L slope prior.} \quad (8c)$$

The first of these imposes a weak prior on the metallicity dependence of the P-L relation. The second imposes a strong prior, effectively eliminating a metallicity dependence of the P-L relation. The last condition is motivated by constraints on the slope of the LMC P-L relation discussed in Section 2.

The results of applying these priors are listed in Table 2. For the R11 rejection, applying these priors drives  $H_0$  downwards by  $\sim 1.5 \text{ km s}^{-1} \text{ Mpc}^{-1}$ . The results for the  $T = 2.25$  rejection are, however, extremely stable to the imposition of the priors.

To determine a final ‘best-estimate’ of  $H_0$  using NGC 4258 as an anchor, I have averaged the  $H_0$  values of fits 3, 7, 11, and added the scatter between these estimates in quadrature with the largest of the error estimates. I have also added a  $1 \text{ km s}^{-1} \text{ Mpc}^{-1}$  error to account for systematics associated with the SNe magnitudes and light curve fitting. This gives

$$H_0 = 70.6 \pm 3.3 \text{ km s}^{-1} \text{ Mpc}^{-1}, \quad \text{NGC 4258.} \quad (9)$$

This value is lower than the value  $H_0 = 72 \pm 3 \text{ km s}^{-1} \text{ Mpc}^{-1}$  quoted by H13 using the revised maser distance to NGC 4258. This difference is caused mainly by the use of difference outlier rejection criteria and the imposition of a metallicity prior. Note also that (9) is within  $1\sigma$  of the *Planck* value of  $H_0$  for the base  $\Lambda$ CDM model.

## 4 USING THE LMC AND MILKY WAY CEPHEIDS AS ANCHORS

### 4.1 The LMC Cepheids

Since the mean metallicities of NGC 4258 and SNe hosts are similar ( $12 + \log(O/H) \approx 8.9$ ), the metallicity dependence discussed in Section 3.2 has a small but non-negligible effect on  $H_0$  if NGC 4258 is used as a distance anchor. However, if we use the LMC as an anchor (for which we assume  $12 + \log(O/H) = 8.5$ ), the metallicity dependence of the P-L relation becomes significant. Values as large as  $Z_W \sim -0.3 \text{ mag dex}^{-1}$  lead to a substantial reduction in the value of  $H_0$  compared to fits in which  $Z_W$  is constrained to be zero (see Table 3).

For the LMC distance, I use the new eclipsing binary distance of  $49.97 \pm 1.13 \text{ kpc}$  determined by Pietrzyński *et al.* (2013). I minimise the sum of the  $\chi^2$  of equations (3) and (6) (which are denoted  $\chi_{\text{LMC}}^2$  and  $\chi_{\text{WFC3}}^2$  respectively) with respect to the parameters of the P-L relation applying the rejection criteria described in Section 3.1 to the R11 Cepheids. The LMC Cepheid sample is as described in Section 2 and  $\sigma_{\text{int,LMC}}$  is kept fixed at 0.113. In applying the  $T = 2.5$  and  $T = 2.25$  rejection criteria,  $\sigma_{\text{int,WFC3}}$  is adjusted to maintain  $\hat{\chi}_{\text{WFC3}}^2 = 1$ . In using the LMC (or MW) Cepheids as a distance anchor, the only role of the NGC 4258 Cepheids in determining  $H_0$  is to influence the slope and metallicity dependence of the global fit to the P-L relation. I have chosen to retain the NGC 4258 Cepheids (as did R11), though the results are very similar if these Cepheids are excluded.

Table 3 lists the results for the three rejection criteria. If no priors are included, the values of  $H_0$  show some sensitivity to the rejection algorithm. This sensitivity is caused by the low metallicity Cepheids in the R11 sample, which pull  $Z_W$  towards negative values (less strongly for the R11 rejection algorithm). Applying the strong metallicity prior, we find very little sensitivity to the rejection algorithm. Furthermore, imposing the slope prior of (8c) has very little effect on the solutions because the slopes of the global fits are well constrained by the LMC Cepheids. Averaging the results for fits 15, 19 and 23, we find:

Global fits: LMC anchor										
Fit	$N_{\text{fit}}$	$\hat{\chi}_{\text{WFC3}}^2$	$H_0$	T=2.5 Rejection			$Z_w$	$\sigma_{\text{int}}$	Priors	
				$p_W$	$b_W$				$Z_w$	$b_W$
13	479	1.00	68.6 (3.5) (2.2)	15.59 (0.08)	-3.23 (0.05)	-0.47 (0.14)	0.32	N	N	
14	478	1.00	69.7 (3.4) (2.1)	15.64 (0.08)	-3.23 (0.05)	-0.35 (0.13)	0.32	W	N	
15	481	1.00	73.5 (2.9) (1.9)	15.76 (0.06)	-3.21 (0.05)	-0.005 (0.020)	0.32	S	N	
16	480	1.00	73.5 (2.8) (1.9)	15.77 (0.06)	-3.22 (0.05)	-0.006 (0.020)	0.32	S	Y	
Fit	$N_{\text{fit}}$	$\hat{\chi}_{\text{WFC3}}^2$	$H_0$	T=2.25 Rejection			$Z_w$	$\sigma_{\text{int}}$	Priors	
				$p_W$	$b_W$				$Z_w$	$b_W$
17	458	1.00	67.4 (3.2) (2.0)	15.57 (0.08)	-3.23 (0.05)	-0.53 (0.13)	0.21	N	N	
18	459	1.00	68.7 (3.2) (2.0)	15.62 (0.08)	-3.23 (0.05)	-0.40 (0.11)	0.22	W	N	
19	447	1.00	73.3 (2.8) (1.8)	15.78 (0.06)	-3.23 (0.05)	-0.007 (0.020)	0.18	S	N	
20	447	1.00	73.3 (2.8) (1.8)	15.78 (0.05)	-3.23 (0.05)	-0.007 (0.020)	0.18	S	Y	
Fit	$N_{\text{fit}}$	$\hat{\chi}_{\text{WFC3}}^2$	$H_0$	R11 Rejection			$Z_w$	$\sigma_{\text{int}}$	Priors	
				$p_W$	$b_W$				$Z_w$	$b_W$
21	390	0.64	70.7 (3.1) (1.8)	15.63 (0.07)	-3.21 (0.04)	-0.31 (0.11)	0.21	N	N	
22	390	0.64	71.3 (3.0) (1.8)	15.64 (0.06)	-3.21 (0.04)	-0.24 (0.10)	0.21	W	N	
23	390	0.65	73.5 (2.7) (1.6)	15.76 (0.05)	-3.21 (0.04)	-0.006 (0.016)	0.21	S	N	
24	390	0.65	73.4 (2.6) (1.5)	15.77 (0.05)	-3.22 (0.04)	-0.006 (0.016)	0.21	S	Y	

Global fits: MW Cepheids anchor										
Fit	$N_{\text{fit}}$	$\hat{\chi}_{\text{WFC3}}^2$	$H_0$	T=2.5 Rejection			$Z_w$	$\sigma_{\text{int}}$	Priors	
				$M_W$	$b_W$				$Z_w$	$b_W$
25	486	1.00	76.5 (4.0) (3.7)	-5.89 (0.05)	-3.22 (0.11)	-0.47 (0.15)	0.30	N	N	
26	484	1.00	77.7 (4.1) (3.8)	-5.88 (0.05)	-3.15 (0.10)	-0.31 (0.13)	0.32	W	N	
27	482	1.00	76.5 (3.9) (3.6)	-5.89 (0.05)	-3.17 (0.11)	-0.006 (0.020)	0.32	S	N	
28	482	1.00	75.7 (3.4) (3.1)	-5.89 (0.05)	-3.20 (0.07)	-0.006 (0.020)	0.32	S	Y	
Fit	$N_{\text{fit}}$	$\hat{\chi}_{\text{WFC3}}^2$	$H_0$	T=2.25 Rejection			$Z_w$	$\sigma_{\text{int}}$	Priors	
				$M_W$	$b_W$				$Z_w$	$b_W$
29	458	1.00	75.2 (3.8) (3.5)	-5.90 (0.05)	-3.26 (0.10)	-0.53 (0.13)	0.21	N	N	
30	459	1.00	74.8 (3.7) (3.5)	-5.90 (0.05)	-3.26 (0.10)	-0.40 (0.11)	0.22	W	N	
31	459	1.00	73.6 (3.6) (3.3)	-5.90 (0.05)	-3.26 (0.10)	-0.009 (0.020)	0.23	S	N	
32	447	1.00	74.7 (3.2) (2.9)	-5.90 (0.05)	-3.24 (0.07)	-0.007 (0.020)	0.18	S	Y	
Fit	$N_{\text{fit}}$	$\hat{\chi}_{\text{WFC3}}^2$	$H_0$	R11 Rejection			$Z_w$	$\sigma_{\text{int}}$	Priors	
				$M_W$	$b_W$				$Z_w$	$b_W$
33	390	0.64	77.9 (3.3) (2.9)	-5.88 (0.04)	-3.15 (0.08)	-0.32 (0.11)	0.21	N	N	
34	390	0.64	77.4 (3.3) (2.9)	-5.88 (0.04)	-3.16 (0.08)	-0.24 (0.10)	0.21	W	N	
35	390	0.65	76.0 (3.2) (2.8)	-5.89 (0.04)	-3.18 (0.08)	-0.006 (0.016)	0.21	S	N	
36	390	0.65	75.4 (2.8) (2.4)	-5.89 (0.04)	-3.21 (0.06)	-0.006 (0.016)	0.21	S	Y	

**Table 3.** As in Table 2, the numbers in brackets give the  $1\sigma$  errors on the parameters computed from the diagonals of the inverse covariance matrix. For  $H_0$  the first number in brackets adds the errors arising from the distance anchors and SNe magnitudes. The second number in brackets lists the error in  $H_0$  from the P-L relation alone.  $N_{\text{fit}}$  gives the number of R11 Cepheids retained in the fits. The remaining columns are as defined in Table 3.

$$H_0 = 73.4 \pm 3.1 \text{ km s}^{-1}\text{Mpc}^{-1}, \quad \text{LMC, strong metallicity prior.} \quad (10)$$

More generally, the solutions of Table 3 show a strong sensitivity to the metallicity dependence of the P-L relation:

$$H_0 \approx (73.4 + 10Z_w) \text{ km s}^{-1}\text{Mpc}^{-1}. \quad (11)$$

An accurate determination of  $H_0$  using the LMC as an anchor therefore requires a precise determination of  $Z_w$ . As discussed in Section 3.2, the strong metallicity dependence at H-band wavelengths derived from the R11 data conflict with the weak metallicity dependence of equation (7). Applying the strong metallicity prior (10),  $H_0$  is in tension, at about the  $1.9\sigma$ , level with the *Planck* base  $\Lambda$ CDM value for  $H_0$ . This tension can be relieved if the metallicity dependence of the P-L relation is somewhat stronger than implied by equation (7).

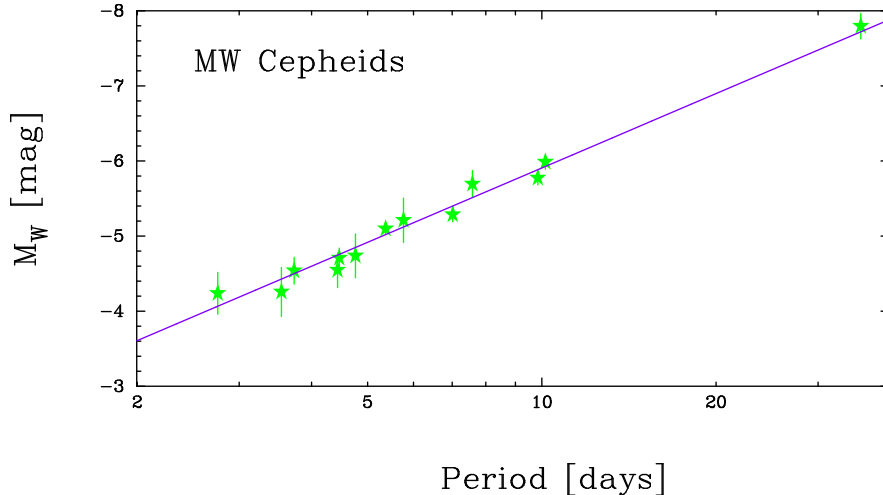


**Figure 4.** Period-luminosity relation for 13 MW Cepheids with parallax measurements (from van Leeuwen *et al.* 2007). The line shows the best fit of (12)

## 4.2 The MW Cepheids

I use the sample of 13 MW Cepheids with parallax measurements and photometry as listed in van Leeuwen *et al.* (2007) (eliminating Polaris). The Wesenheit P-L relation (HVI photometry) for these Cepheids is shown in Figure 5. A fit to these gives

$$M_W = -5.91 \pm 0.17, \quad b_W = -3.29 \pm 0.17, \quad \hat{\chi}^2 = 0.57, \quad (12)$$

where  $M_W$  replaces  $A$  in equation (1). Note that the slope is not well constrained because of the dearth of Cepheids with periods greater than 10 days in this small sample. The slope is, however, compatible with the slope determined from the LMC Cepheids. The reduced  $\chi^2$  of this sample is smaller than unity, but because of the small sample size this is not statistically significant and leaves room for a significant ‘internal dispersion’ (which cannot be well constrained from  $\hat{\chi}^2$ ). In the fits below, I adopt an internal dispersion of  $\sigma_{int} = 0.10$ , consistent with the internal dispersion of the LMC sample. The parameters of the MW Cepheid fits discussed below are insensitive to this value, though adopting  $\sigma_{int} = 0.10$  has the effect of slightly downweighting the MW Cepheids compared to the LMC and/or NGC 4258 when combining distance anchors.

The global fits using the MW parallax distances are summarized in Table 3. The metallicity dependences of these fits are skewed by the low metallicity outliers in the R11 sample. These raise  $H_0$  and introduce a sensitivity to the outlier rejection algorithm. Imposing the strong metallicity and P-L slope priors reduces the sensitivity to these outliers. Averaging the results of fits 28, 32 and 36 gives

$$H_0 = 75.3 \pm 3.5 \text{ km s}^{-1}\text{Mpc}^{-1}, \quad \text{MW, strong metallicity and slope priors.} \quad (13)$$

This result is in tension at about the  $2.1\sigma$ , level with the *Planck* base  $\Lambda$ CDM value for  $H_0$ . Because of the small size of the MW Cepheid sample, the instability strip is not well sampled. In addition, the lack of overlap between the periods of the MW Cepheids and the R11 sample leads to a sensitivity of  $H_0$  to the slope prior and to the choice of period range for the R11 Cepheids (see Appendix A). Coupled with possible systematic errors associated with matching ground-based and HST photometry, I consider the MW Cepheids to be the least reliable of the three distance anchors.

## 5 COMBINING DISTANCE ANCHORS

### 5.1 Joint solutions

Whereas R11 found similar values of  $H_0$  using NGC 4258 and the MW Cepheids as distance anchors, with  $H_0$  for the LMC lying low, we find reasonable agreement between the  $H_0$  values for the LMC and MW Cepheids (equations 10 and 13) with  $H_0$  for NGC 4258 lying low (equation 9). There are two reasons why our results differ from R11. Firstly, the revised megamaser distance to NGC 4258 of H13 lowers  $H_0$  by about  $3 \text{ km s}^{-1}\text{Mpc}^{-1}$ . Secondly, we have argued that the strong metallicity dependence of the global fits is caused by sub-luminous outliers in the P-L relation, and may be unphysical. Imposing a strong metallicity prior centred around  $Z_W = 0$  raises the LMC solutions for  $H_0$  substantially. A further difference between R11



Global fits: NGC 4258+LMC anchors

Fit	$N_{\text{fit}}$	$\hat{\chi}_{\text{WFC3}}^2$	$H_0$	T=2.5 Rejection			$\sigma_{\text{int}}$	Priors	
				$M_W$	$b_W$	$Z_w$		$Z_w$	$b_W$
37	477	1.00	69.3 (2.4)	-6.10 (0.06)	-3.22 (0.05)	-0.45 (0.13)	0.30	N	N
38	478	1.00	69.8 (2.4)	-6.07 (0.06)	-3.22 (0.05)	-0.35 (0.11)	0.30	W	N
39	477	1.00	71.4 (2.4)	-5.99 (0.05)	-3.23 (0.05)	-0.009 (0.020)	0.30	S	N
40	477	1.00	71.5 (2.4)	-5.99 (0.05)	-3.24 (0.05)	-0.009 (0.020)	0.30	S	Y

Fit	$N_{\text{fit}}$	$\hat{\chi}_{\text{WFC3}}^2$	$H_0$	T=2.25 Rejection			$\sigma_{\text{int}}$	Priors	
				$M_W$	$b_W$	$Z_w$		$Z_w$	$b_W$
41	458	1.00	69.0 (2.3)	-6.10 (0.06)	-3.23 (0.05)	-0.48 (0.12)	0.21	N	N
42	459	1.00	69.4 (2.3)	-6.07 (0.06)	-3.23 (0.05)	-0.38 (0.11)	0.22	W	N
43	448	1.00	71.8 (2.3)	-5.97 (0.05)	-3.24 (0.05)	-0.009 (0.020)	0.18	S	N
44	448	1.00	71.9 (2.3)	-5.97 (0.05)	-3.23 (0.04)	-0.009 (0.020)	0.18	S	Y

Fit	$N_{\text{fit}}$	$\hat{\chi}_{\text{WFC3}}^2$	$H_0$	R11 Rejection			$\sigma_{\text{int}}$	Priors	
				$M_W$	$b_W$	$Z_w$		$Z_w$	$b_W$
45	390	0.64	71.0 (1.9)	-6.06 (0.05)	-3.21 (0.04)	-0.29 (0.10)	0.21	N	N
46	390	0.64	71.2 (1.9)	-6.04 (0.05)	-3.21 (0.04)	-0.24 (0.09)	0.21	W	N
47	390	0.66	72.1 (1.9)	-5.98 (0.04)	-3.22 (0.04)	-0.008 (0.016)	0.21	S	N
48	390	0.65	72.1 (1.9)	-5.98 (0.04)	-3.22 (0.04)	-0.008 (0.016)	0.21	S	Y

Global fits: NGC 4258+MW Cepheid anchors

Fit	$N_{\text{fit}}$	$\hat{\chi}_{\text{WFC3}}^2$	$H_0$	T=2.5 Rejection			$\sigma_{\text{int}}$	Priors	
				$M_W$	$b_W$	$Z_w$		$Z_w$	$b_W$
49	476	1.00	72.2 (2.9)	-5.96 (0.05)	-3.31 (0.09)	-0.51 (0.14)	0.29	N	N
50	478	1.00	71.7 (2.9)	-5.96 (0.05)	-3.32 (0.09)	-0.35 (0.13)	0.30	W	N
51	477	1.00	70.9 (2.8)	-5.96 (0.05)	-3.32 (0.09)	-0.007 (0.020)	0.30	S	N
52	477	1.00	71.6 (2.6)	-5.96 (0.05)	-3.28 (0.07)	-0.007 (0.020)	0.30	S	Y

Fit	$N_{\text{fit}}$	$\hat{\chi}_{\text{WFC3}}^2$	$H_0$	T=2.25 Rejection			$\sigma_{\text{int}}$	Priors	
				$M_W$	$b_W$	$Z_w$		$Z_w$	$b_W$
53	456	1.00	72.1 (2.8)	-5.95 (0.06)	-3.32 (0.09)	-0.51 (0.12)	0.21	N	N
54	455	1.00	71.4 (2.7)	-5.95 (0.05)	-3.34 (0.09)	-0.38 (0.11)	0.21	W	N
55	447	1.00	71.5 (2.7)	-5.94 (0.05)	-3.30 (0.08)	-0.007 (0.020)	0.18	S	N
56	448	1.00	72.2 (2.5)	-5.95 (0.05)	-3.27 (0.05)	-0.007 (0.020)	0.19	S	Y

Fit	$N_{\text{fit}}$	$\hat{\chi}_{\text{WFC3}}^2$	$H_0$	R11 Rejection			$\sigma_{\text{int}}$	Priors	
				$M_W$	$b_W$	$Z_w$		$Z_w$	$b_W$
57	390	0.65	73.8 (2.3)	-5.95 (0.04)	-3.23 (0.07)	-0.30 (0.11)	0.21	N	N
58	390	0.64	73.5 (2.3)	-5.95 (0.04)	-3.24 (0.07)	-0.23 (0.07)	0.21	W	N
59	390	0.66	72.6 (2.3)	-5.95 (0.04)	-3.25 (0.07)	-0.006 (0.016)	0.21	S	N
60	390	0.66	72.7 (2.1)	-5.95 (0.04)	-3.24 (0.05)	-0.006 (0.016)	0.21	S	Y

Global fits: LMC+MW Cepheid anchors

Fit	$N_{\text{fit}}$	$\hat{\chi}_{\text{WFC3}}^2$	$H_0$	T=2.5 Rejection			$\sigma_{\text{int}}$	Priors	
				$M_W$	$b_W$	$Z_w$		$Z_w$	$b_W$
61	479	1.00	72.4 (2.5)	-5.98 (0.05)	-3.25 (0.05)	-0.30 (0.12)	0.31	N	N
62	479	1.00	72.6 (2.5)	-5.96 (0.05)	-3.25 (0.05)	-0.24 (0.11)	0.31	W	N
63	480	1.00	74.1 (2.5)	-5.92 (0.05)	-3.23 (0.05)	-0.005 (0.020)	0.32	S	N
64	477	1.00	74.1 (2.5)	-5.92 (0.05)	-3.23 (0.04)	-0.005 (0.020)	0.32	S	Y

Fit	$N_{\text{fit}}$	$\hat{\chi}_{\text{WFC3}}^2$	$H_0$	T=2.25 Rejection			$\sigma_{\text{int}}$	Priors	
				$M_W$	$b_W$	$Z_w$		$Z_w$	$b_W$
65	459	1.00	71.6 (2.4)	-5.99 (0.05)	-3.26 (0.05)	-0.36 (0.11)	0.21	N	N
66	455	1.00	71.9 (2.4)	-5.97 (0.05)	-3.26 (0.05)	-0.28 (0.10)	0.21	W	N
67	448	1.00	73.6 (2.4)	-5.92 (0.05)	-3.24 (0.05)	-0.007 (0.020)	0.18	S	N
68	448	1.00	73.7 (2.4)	-5.92 (0.05)	-3.24 (0.04)	-0.007 (0.020)	0.18	S	Y

Fit	$N_{\text{fit}}$	$\hat{\chi}_{\text{WFC3}}^2$	$H_0$	R11 Rejection			$\sigma_{\text{int}}$	Priors	
				$M_W$	$b_W$	$Z_w$		$Z_w$	$b_W$
69	390	0.64	73.4 (2.0)	-5.96 (0.04)	-3.23 (0.04)	-0.20 (0.09)	0.21	N	N
70	390	0.65	73.6 (2.0)	-5.95 (0.04)	-3.23 (0.04)	-0.16 (0.09)	0.21	W	N
71	390	0.65	74.1 (2.0)	-5.92 (0.04)	-3.23 (0.04)	-0.005 (0.016)	0.21	S	N
72	390	0.65	74.0 (2.0)	-5.92 (0.04)	-3.23 (0.04)	-0.006 (0.016)	0.21	S	Y

Table 4. Solutions combining distance anchors. The columns are as defined in Tables 2 and 3.

Global fits: NGC 4258+LMC+MW Cepheids anchor

Fit	$N_{\text{fit}}$	$\tilde{\chi}_{\text{WFC3}}^2$	$H_0$	T=2.5 Rejection			$\sigma_{\text{int}}$	Priors	
				$M_W$	$b_W$	$Z_w$		$Z_w$	$b_W$
73	479	1.00	71.5 (2.2)	-6.00 (0.04)	-3.26 (0.05)	-0.33 (0.12)	0.30	N	N
74	479	1.00	71.6 (2.3)	-5.99 (0.04)	-3.26 (0.05)	-0.27 (0.11)	0.31	W	N
75	477	1.00	72.3 (2.3)	-5.95 (0.04)	-3.26 (0.05)	-0.008 (0.020)	0.30	S	N
76	477	1.00	72.4 (2.2)	-5.95 (0.04)	-3.25 (0.04)	-0.008 (0.020)	0.30	S	Y
Fit	$N_{\text{fit}}$	$\tilde{\chi}_{\text{WFC3}}^2$	$H_0$	T=2.25 Rejection			$\sigma_{\text{int}}$	Priors	
				$M_W$	$b_W$	$Z_w$		$Z_w$	$b_W$
77	455	1.00	71.3 (2.2)	-5.99 (0.04)	-3.26 (0.05)	-0.34 (0.11)	0.21	N	N
78	455	1.00	71.4 (2.2)	-5.98 (0.04)	-3.26 (0.05)	-0.29 (0.10)	0.21	W	N
79	447	1.00	72.4 (2.2)	-5.94 (0.04)	-3.25 (0.05)	-0.007 (0.020)	0.18	S	N
80	447	1.00	72.5 (2.2)	-5.94 (0.04)	-3.25 (0.04)	-0.007 (0.020)	0.18	S	Y
Fit	$N_{\text{fit}}$	$\tilde{\chi}_{\text{WFC3}}^2$	$H_0$	R11 Rejection			$\sigma_{\text{int}}$	Priors	
				$M_W$	$b_W$	$Z_w$		$Z_w$	$b_W$
81	390	0.64	72.6 (1.8)	-5.98 (0.03)	-3.24 (0.04)	-0.22 (0.09)	0.21	N	N
82	390	0.65	72.6 (1.8)	-5.97 (0.03)	-3.24 (0.04)	-0.18 (0.08)	0.21	W	N
83	390	0.66	72.9 (1.8)	-5.95 (0.03)	-3.24 (0.04)	-0.006 (0.016)	0.21	S	N
84	390	0.66	72.9 (1.8)	-5.95 (0.03)	-3.24 (0.04)	-0.006 (0.016)	0.21	S	Y

**Table 4. (contd.)** Solutions combining distance anchors.

results and the results presented here is that our errors on  $H_0$  are larger. This is most noticeable for the MW solutions in Table 3.

To account for correlated errors between ground-based and HST photometry and correlated errors between the SNe magnitudes, I minimise:

$$\chi^2 = \sum_{ij,j=1-9} \frac{(m_{W,ij} - m_{W,i}^P)^2}{(\sigma_{e,ij}^2 + \sigma_{\text{int}}^2)} + (m_{W,i} - m_W^P)(C^{\text{LMC+MW}})_{ij}^{-1}(m_{w,j} - m_W^P) + (m_{V,i} - m_V^P)(C^{\text{SNe}})_{ij}^{-1}(m_{V,j} - m_V^P) + \frac{(\mu_{0,4258} - \mu_{0,4258}^M)^2}{\sigma_{\mu_{0,4258}}^2} + \frac{(\mu_{0,\text{LMC}} - \mu_{0,\text{LMC}}^M)^2}{\sigma_{\mu_{0,\text{LMC}}}^2}. \quad (14)$$

The first term is summed over the R11 Cepheids as in equation (6). The second term is summed over the LMC and MW Cepheids, where the covariance matrix  $C^{\text{LMC,MW}}$  is

$$C_{ij}^{\text{LMC,MW}} = (\sigma_i^2 + \sigma_{\text{int}}^2)\delta_{ij} + \sigma_{\text{cal}}^2, \quad (15)$$

where  $\sigma_i$  is the magnitude error,  $\sigma_{\text{int}}$  is the internal scatter, and  $\sigma_{\text{cal}}$  is the calibration error between the ground based and WFC3 photometry (assumed to be  $\sigma_{\text{cal}} = 0.04$  mag. as in R11). The third term is summed over the SNe magnitudes  $m_{V,i}$  and the covariance matrix  $C^{\text{SNe}}$  is

$$C_{ij}^{\text{SNe}} = (\sigma_i^2)\delta_{ij} + \sigma_{5a_V}^2, \quad (16)$$

where  $\sigma_i$  is the SNe magnitude error and  $\sigma_{5a_V}$  is the error in  $5a_V$ , where  $a_V$  is the intercept of the SNe Ia magnitude-redshift relation ( $\sigma_{5a_V} = 0.01005$ , from R11). Finally,  $\mu_{0,4258}$  and  $\mu_{0,\text{LMC}}$  are the distance moduli of NGC 4258 and the LMC,  $\mu_{0,4258}^M$  and  $\mu_{0,\text{LMC}}^M$  are their measured values (from the maser and eclipsing binary distances respectively) with errors  $\sigma_{\mu_{0,4258}}$  and  $\sigma_{\mu_{0,\text{LMC}}}$ . The theoretically predicted magnitudes are

$$\text{SNe hosts : } m_{ij}^P = \mu_{0,i} + M_W + b_W(\log P_{ij} - 1) + Z_W \Delta \log(\text{O/H})_{ij}, \quad (17a)$$

$$\text{NGC 4258 : } m_j^P = \mu_{0,4258} + M_W + b_W(\log P_j - 1) + Z_W \Delta \log(\text{O/H})_j, \quad (17b)$$

$$\text{LMC : } m_j^P = \mu_{0,\text{LMC}} + M_W + b_W(\log P_j - 1) + Z_W \Delta \log(\text{O/H})_j, \quad (17c)$$

$$\text{MW : } m_j^P = M_W + b_W(\log P_j - 1) + Z_W \Delta \log(\text{O/H})_j, \quad (17d)$$

$$\text{SNe : } m_{V,i}^P = \mu_{0,i} + 5 \log H_0 - 25 - 5a_V. \quad (17e)$$

Results for joint distance anchor fits are given in Table 4. There are several points worth noting:

- As in the analyses presented in previous Sections, the low metallicity Cepheid outliers in the R11 data lead to a sensitivity to the outlier rejection criterion.
- With no metallicity or slope priors, the combined solutions using NGC 4258 + LMC anchors are discrepant at  $\gtrsim 2\sigma$  with the MW anchor solutions given in Table 3. (Compare, for example, the results for fits 33 and 45.)
- Applying a strong metallicity prior, the solutions for  $H_0$  for the combined NGC 4258 and LMC fits become insensitive to the outlier rejection criteria (and are consistent to within  $\sim 0.5 \text{ km s}^{-1} \text{ Mpc}^{-1}$ ).

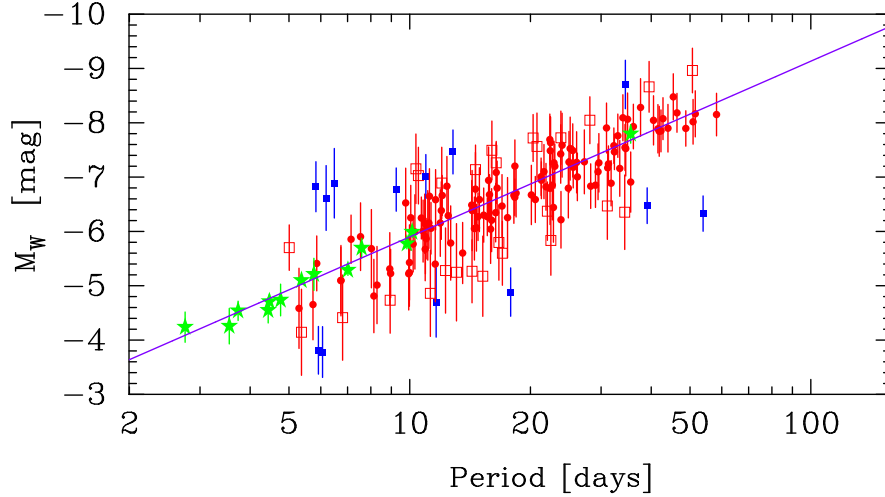


**Figure 5.** Period-luminosity fit used to determine the distance modulus to NGC 4258 using the MW Cepheids as a distance anchor. The MW Cepheids are shown by the (green) filled stars. The rest of the points (red and blue) show the R11 Cepheids. As in Figure 2, filled (red) circles are accepted by both the R11 and  $T = 2.25$  rejection criteria while filled (blue) squares are rejected by both criteria. Open (red) squares are rejected by R11 but accepted by the  $T = 2.25$  criterion. The line shows the best fit P-L relation.

- Since the slope of the P-L relation is well constrained by the LMC Cepheids, adding a slope prior has almost no effect on solutions that include the LMC Cepheids.

If we accept each of these distance anchors at face value, and average over the outlier rejection criteria as in the previous Section using the solutions with strong metallicity and no slope priors for (18a) and (18d) and strong metallicity and slope priors for (18b) and (18c), then we find:

$$H_0 = 71.8 \pm 2.6 \text{ km s}^{-1} \text{Mpc}^{-1}, \quad \text{NGC 4258 + LMC}, \quad (18a)$$

$$H_0 = 72.2 \pm 2.8 \text{ km s}^{-1} \text{Mpc}^{-1}, \quad \text{NGC 4258 + MW}, \quad (18b)$$

$$H_0 = 73.9 \pm 2.7 \text{ km s}^{-1} \text{Mpc}^{-1}, \quad \text{LMC + MW}, \quad (18c)$$

$$H_0 = 72.5 \pm 2.5 \text{ km s}^{-1} \text{Mpc}^{-1}, \quad \text{NGC 4258 + LMC + MW}. \quad (18d)$$

These values differ by  $1.6\sigma$ ,  $1.6\sigma$ ,  $2.2\sigma$  and  $1.9\sigma$  respectively from the *Planck* value of  $H_0$  for the base  $\Lambda$ CDM model. Evidently, using the LMC and especially the MW Cepheids as distance anchors pulls  $H_0$  to higher values than those derived using the megamaser distance. Note that when R11 combine all three distance anchors, they conservatively adopt the largest error from any pair of distance anchors. Adopting the same approach would increase the error in (18d) to  $2.8 \text{ km s}^{-1} \text{Mpc}^{-1}$ .

## 5.2 Consistency of distance anchors

Before accepting (18a) - (18d) it is worth investigating internal consistency tests of the three distance anchors. We first use the MW Cepheids to compute the distance modulus to the LMC assuming no metallicity dependence of the P-L relation. The result is

$$\mu_{0,LMC} = 18.455 \pm 0.042, \quad (19)$$

in good agreement with the Pietrzyński *et al.* (2013) eclipsing binary distance modulus of  $18.493 \pm 0.049$ . In fact, combining these estimates we deduce

$$Z_W = 0.10 \pm 0.16 \text{ mag. dex}^{-1}, \quad (20)$$

consistent with a weak metallicity dependence of the P-L relation at H-band.

Next, we use the LMC Cepheids to determine a distance modulus to NGC 4258, assuming the Pietrzyński *et al.* (2013) eclipsing binary distance. This solution is based on the likelihood of equation (14). I impose the strong metallicity prior and average over the three outlier rejection criteria, adding the scatter to the final error estimate. The result is

$$\mu_{0,4258} = 29.285 \pm 0.083, \quad (21)$$

which is within  $1.1\sigma$  of the H13 megamaser distance modulus of  $29.404 \pm 0.066$ . Combining these estimates we deduce

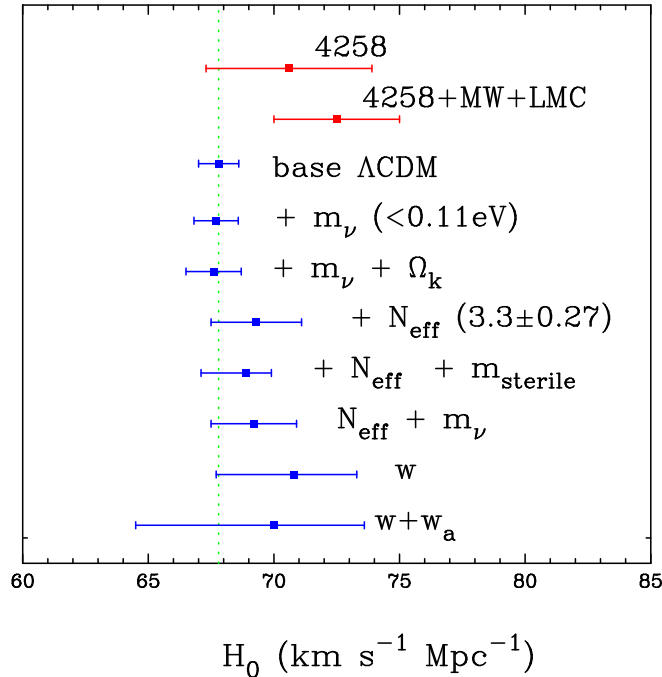


**Figure 6.** The direct estimates (red) of  $H_0$  (together with  $1\sigma$  error bars) for the NGC 4258 distance anchor (equation 9) and for all three distance anchors (equation 18d). The remaining (blue) points show the constraints from P13 for the base  $\Lambda$ CDM cosmology and some extended models combining CMB data with data from baryon acoustic oscillation surveys. The extensions are as follows:  $m_\nu$ , the mass of a single neutrino species;  $m_\nu + \Omega_k$ , allowing a massive neutrino species and spatial curvature;  $N_{\text{eff}}$ , allowing additional relativistic neutrino-like particles;  $N_{\text{eff}} + m_{\text{sterile}}$ , adding a massive sterile neutrino and additional relativistic particles;  $N_{\text{eff}} + m_\nu$ , allowing a massive neutrino and additional relativistic particles;  $w$ , dark energy with a constant equation of state  $w = p/\rho$ ;  $w + w_a$ , dark energy with a time varying equation of state. I give the  $1\sigma$  upper limit on  $m_\nu$  and the  $1\sigma$  range for  $N_{\text{eff}}$ . See P13 for further details on these extended models.

$$Z_W = -0.29 \pm 0.26 \text{ mag. dex}^{-1}, \quad (22)$$

consistent with zero but with even lower precision than the estimate of (20).

Finally, I use the MW Cepheids to compute a distance modulus to NGC 4258. Since the MW Cepheids have similar metallicities to the mean of the Cepheids in NGC 4258, uncertainties in the metallicity dependence of the P-L relation do not introduce a significant source of error into the distance modulus. Nevertheless, I impose the strong metallicity prior on the solutions and average over the three outlier criteria. This gives

$$\mu_{0,4258} = 29.241 \pm 0.079, \quad (23)$$

which is about  $1.6\sigma$  lower than the H13 distance modulus. Figure 5 shows the  $T = 2.25$  fit to the MW and NGC 4258 Cepheids.

The differences between the  $H_0$  values for the three distance anchors are reflected by these differences in the distance moduli of NGC 4258. The MW and LMC Cepheids (assuming zero metallicity dependence) give a shorter distance to NGC 4258 than the H13 revised megamaser distance. It is possible that the true distance to NGC 4258 is substantially lower than the H13 central value. However, it is also possible that the tension is caused by a more subtle effect, for example, a residual  $\sim 0.1$  mag. bias of the NGC 4258 P-L relation caused by asymmetric outliers or systematic errors in the corrections for crowding biases.

Further work on the tension between (21), (23) and the H13 distance modulus is required to improve on the estimate of (18d). Evidently, the discrepancies are not of high enough statistical significance to reveal an obvious inconsistency between any of the distance anchors. However, the difference between (23) and the H13 distance modulus is quite large and suggestive of a possible problem.

## 6 CONCLUSIONS AND DISCUSSION

The SH0ES project was cleverly designed to minimise the impact of metallicity, crowding, and photometric calibration biases when comparing Cepheids measured in SNe hosts with those in NGC 4258. These methodological reasons argue that higher

weight should be placed on the NGC 4258 anchor than either the LMC or MW anchors when using the R11 data. However, the value of  $H_0$  derived using NGC 4258 as an anchor relies on the fidelity of the geometric maser distance. Despite the extensive VLBI campaign described by H13, systematic errors contribute significantly to the total error in the megamaser distance. It may therefore be dangerous to place very high weight on the NGC 4258 distance without cross-checks with independent distance anchors.

However, in addition to the methodological issues that drove the design of the SH0ES project, there are significant problems in using the LMC and MW distance anchors. Although there are several accurate and consistent eclipsing binary distance estimates to the LMC (Fitzpatrick *et al.* 2002; Ribas *et al.* 2002; Pietrzyński *et al.* 2009, 2013)  $H_0$  derived using the LMC as a distance anchor is extremely sensitive to any metallicity dependence of the P-L relation (equation 11). I show that the R11 sample contains sub-luminous low metallicity Cepheids, pointing either to a stronger than expected metallicity dependence of the near-IR P-L relation (in conflict with the Freedman and Madore 2011 analysis), a possible misidentification of these objects as classical Cepheids, or to some unidentified systematic error in their magnitudes. The presence of these sub-luminous Cepheids causes some sensitivity to the rejection criteria used to identify outliers from the mean P-L relation. However, if a strong metallicity prior is imposed, the global fits and derived values of  $H_0$  become insensitive to the outlier rejection criteria. (It is also worth noting that the strong metallicity prior also affects the value of  $H_0$  derived using NGC 4258 as a distance anchor: we find  $H_0 = 70.6 \pm 3.3 \text{ km s}^{-1}\text{Mpc}^{-1}$  compared to the value  $H_0 = 72.0 \pm 3.0 \text{ km s}^{-1}\text{Mpc}^{-1}$  quoted by H13.) One would have greater confidence in using the LMC anchor if there were stronger observational constraints on  $Z_W$ .

The sample of MW Cepheids with parallax measurements is small and contains only one star that overlaps with the period range sampled by Cepheids in the SNe host galaxies (*cf* Figures 2 and 4). Use of the MW Cepheids as an anchor is therefore susceptible to sample biases and small number statistics. The distance modulus to NGC 4258 derived from the MW Cepheids is lower by about  $1.6\sigma$  compared to the H13 megamaser distance modulus. As a consequence,  $H_0$  derived using the MW Cepheids as a distance anchor is higher than that derived from the megamaser distance and is discrepant by about  $2.2\sigma$  with the *Planck* base  $\Lambda$ CDM value. This is the largest discrepancy reported in this paper with the *Planck* determination of  $H_0$ . Observations with the GAIA satellite will increase the number of Galactic Cepheids with accurate parallaxes into the many thousands. It will be interesting to see whether the tensions with the megamaser distance and with the *Planck* base  $\Lambda$ CDM cosmology persist.

The value of  $H_0$  derived here from the megamaser distance is within  $1\sigma$  of the *Planck* base  $\Lambda$ CDM value of  $H_0$ . Although there are some tensions between the three distance anchors, none are sufficiently compelling to justify excluding either the MW or LMC anchors from a joint fit. Imposing the strong metallicity prior, the combination of all three distance anchors raises  $H_0$  to  $72.5 \pm 2.5 \text{ km s}^{-1}\text{Mpc}^{-1}$ , which is within  $1.9\sigma$  of the *Planck* base  $\Lambda$ CDM value.

Figure 6 compares these two estimates of  $H_0$  with the P13 results from the *Planck*+WP+highL+BAO<sup>3</sup> likelihood for the base  $\Lambda$ CDM cosmology and some extended  $\Lambda$ CDM models. I show the combination of CMB and BAO data since  $H_0$  is poorly constrained for some of these extended models using CMB temperature data alone. (For reference, for this data combination  $H_0 = 67.80 \pm 0.77 \text{ km s}^{-1}\text{Mpc}^{-1}$  in the base  $\Lambda$ CDM model.) The combination of CMB and BAO data is certainly not prejudiced against new physics, yet the  $H_0$  values for the extended  $\Lambda$ CDM models shown in this figure all lie within  $1\sigma$  of the best fit value for the base  $\Lambda$ CDM model. For example, in the models exploring new physics in the neutrino sector, the central value of  $H_0$  never exceeds  $69.3 \text{ km s}^{-1}\text{Mpc}^{-1}$ . If the true value of  $H_0$  lies closer to, say,  $H_0 = 74 \text{ km s}^{-1}\text{Mpc}^{-1}$ , the dark energy sector, which is poorly constrained by the combination of CMB and BAO data, seems a more promising place to search for new physics.

In summary, the discrepancies between the *Planck* results and the direct  $H_0$  measurements shown in Figure 5 are not large enough to provide compelling evidence for new physics beyond the base  $\Lambda$ CDM cosmology.

**Acknowledgements:** I am particularly grateful to Adam Riess, who has answered patiently my many questions on the analysis of the SH0ES data. I also thank Rob Kennicutt, Wendy Freedman and Brian Schmidt for valuable discussions and correspondence and the referee for a helpful report.

## REFERENCES

Battye R., Moss A., 2013, arXiv:1308.5870.  
 Braatz J. *et al.*, 2013, *Advancing the Physics of Cosmic Distances*, Proceedings IAU Symposium, 289, 2012 Cambridge University Press.  
 Courbin F. *et al.*, 2011, *A&A*, 536, 53.  
 Fitzpatrick E. L., Ribas I., Guinan E. F., DeWarf L. E., Maloney F. P., Massa, D., 2002, *ApJ*, 564, 260.  
 Freedman W.L. *et al.*, 2001, *ApJ*, 553, 47.  
 Freedman W.L., Madore B.F., 2010, *ARAA*, 48, 673.  
 Freedman W.L., Madore B.F., 2011, *ApJ*, 734, 46.

<sup>3</sup> *Planck* temperature likelihood combined with the WMAP polarization likelihood at low multipoles combined with high resolution CMB experiments combined with baryon acoustic oscillation (BAO) measurements.

- Freedman W.L., *et al.*, 2011, AJ, 142, 192.  
 Freedman W.L., Madore B.F., Scowcroft V., Burns C., Monson A., Persson S.E., Siebert M., Rigby J., 2012, ApJ, 758, 24.  
 Hamann J, Hasenkamp J., 2013, arXiv:1308.3255.  
 Herrnstein J.R. *et al.*, 1999, Nature, 400, 539.  
 Hinshaw *et al.*, 2012, arXiv/astro-ph:1212.5226.  
 Hou Z. *et al.*, 2012, arXiv/astro-ph:1212.6267.  
 Humphreys E.M.L., Ried M.J., Moran J.M., Greenhill L.J., Argon A.L., 2013, arXiv/astro-ph:1307.7653. (H13)  
 Kennicutt R.C. *et al.*, 1998, ApJ, 498, 181.  
 Macri L.M., Stanek K.Z., Bersier D., Greenhill L.J., Ried M.J., 2006, ApJ, 652, 1133.  
 McGonegal R., McAlary C.W., Madore B.F., McLaren R.A., 1982, ApJL, 257, L33.  
 Ngeow C., Kanbur S.M., Neislon H.R., Nanthakumar A., Buonaccorsi J, 2009, ApJ, 693, 691.  
 Persson S.E., Madore B.F., Krzemiński W., Freedman W.L., Roth M., Murphey D.C., 2004, AJ, 128, 2239.  
 Pietrzyński G. *et al.*, 2009, ApJ, 695, 862.  
 Pietrzyński G. *et al.*, 2013, Nature, 495, 75.  
 Planck Collaboration 2013, arXiv:1303.5076.  
 Ribas I., Fitzpatrick E.L., Maloney F.P., Guinan E.F., Udalski A., 2002, ApJ, 574, 771.  
 Reid M. J., Braatz J. A., Condon J. J., Lo K. Y., Kuo C. Y., Impellizzeri C. M. V., Henkel, C., 2013, ApJ, 767, 154.  
 Rest A. *et al.*, 2013, arXiv:1310.3828.  
 Riess A. *et al.*, 2009, ApJ, 699, 539.  
 Riess A. *et al.*, 2011, ApJ, 730, 119. (R11)  
 Riess A. *et al.*, 2012, ApJ, 752, 26.  
 Romaniello M. *et al.*, 2008, A&A, 488, 731.  
 Sakai K.M. *et al.*, 2004, ApJ, 608, 42.  
 Scowcroft V., Bersier D., Mould J.R., Wood P.R., 2009, arXiv:0903.4088.  
 Scowcroft V., Freedman W.L., Madore B.F., Monson A.J., Persson S.E., Seibert M., Rigby J.R., Sturch L., 2011, ApJ, 743, 76.  
 Scowcroft V., Freedman W.L., Madore B.F., Monson A.J., Persson S.E., Seibert M., Rigby J., Melbourne J., 2013, ApJ, 773, 106.  
 Sebo K.M. *et al.*, 2002, ApJS, 142, 71.  
 Tewes M. *et al.*, 2013, A&A, 556, 22.  
 Suyu S.H. *et al.*, 2010, ApJ, 711, 201.  
 Suyu S.H. *et al.*, 2013, arXiv:1306.4732.  
 Sievers J.L. *et al.*, 2013, arXiv:1301.0824.  
 Tammann G.A., Sandage A., Reindle B., 2008, ARAA, 15, 289.  
 van Leeuwen F., Feast M.W., Whitelock P.A., Laney C.D., 2007, MNRAS, 379, 723.  
 Wyman M., Rudd D.H., Vanderveld R.A., Hu W., 2013, arXiv:1307.7715.

## APPENDIX A: EXTENDING THE PERIOD RANGE OF THE GLOBAL FITS

Throughout this paper, I imposed an upper period limit of 60 days on the R11 Cepheid sample. As noted in Section 2, there is evidence from analyses of LMC Cepheids that the P-L relation flattens for Cepheids with periods  $> 60$  days (Persson *et al.*, 2004; Freedman *et al.* 2011; Scowcroft *et al.* 2011). R11, however, used all Cepheids with periods  $< 205$  days in their analysis. The purpose of this Appendix is to show how the results of Sections 3 and 4 change if the Cepheid period range is extended. Table A1 is the equivalent of Tables 2 and 3, but using R11 Cepheids with periods  $< 205$  days. The main change is that the slopes of the P-L relation in many of the fits become substantially flatter than the LMC slopes of equation (4). As a consequence, the global fits in Table A1 become more sensitive to the imposition of an LMC slope prior, whereas the fits in Tables 2 and 3 are insensitive to the slope prior. This is particularly true for fits A25-A36 using the MW Cepheids as an anchor. Without any slope prior,  $H_0$  is about  $80 \text{ km s}^{-1} \text{ Mpc}^{-1}$  and is inconsistent with  $H_0$  determined using the maser distance to NGC 4258 (fits A1-A12). This provides further evidence that the MW Cepheids are the least reliable of the three distance anchors. R11 adopted a slope prior of  $-3.3 \pm 0.1$  in their fits involving MW Cepheids. This prior is, however, inconsistent with the shallower slopes of the SNe host galaxy P-L relations derived using Cepheids with periods up to 205 days.

Comparing Table A1 with Tables 2 and 3, we see that the flatter slopes of the P-L relation have little impact on  $H_0$  using either NGC 4258 or the LMC Cepheids as a distance anchor. However, adopting an upper period of limit of 60 days, as in the main body of this paper, all of the P-L slopes are consistent with the LMC P-L relation. The global fits are then insensitive to the imposition of an LMC slope prior (even for the MW Cepheids).

Global fits: NGC 4258 anchor

Fit	$N_{\text{fit}}$	$\hat{\chi}_{\text{WF3}}^2$	$H_0$	T=2.5 Rejection			$\sigma_{\text{int}}$	Priors	
				$p_W$	$b_W$	$Z_w$		$Z_w$	$b_W$
A1	552	1.00	71.5 (3.1) (2.2)	26.08 (0.12)	-2.88 (0.08)	-0.33 (0.14)	0.30	N	N
A2	550	1.00	71.6 (3.1) (2.2)	26.09 (0.12)	-2.88 (0.08)	-0.21 (0.12)	0.29	W	N
A3	551	1.00	71.0 (3.0) (2.1)	26.12 (0.12)	-2.91 (0.08)	-0.005 (0.020)	0.30	S	N
A4	551	1.00	69.2 (2.9) (2.0)	26.33 (0.09)	-3.06 (0.06)	-0.004 (0.020)	0.31	S	Y

Fit	$N_{\text{fit}}$	$\hat{\chi}_{\text{WF3}}^2$	$H_0$	T=2.25 Rejection			$\sigma_{\text{int}}$	Priors	
				$p_W$	$b_W$	$Z_w$		$Z_w$	$b_W$
A5	523	1.00	72.0 (2.9) (2.0)	26.21 (0.10)	-2.95 (0.07)	-0.46 (0.12)	0.21	N	N
A6	524	1.00	71.7 (2.9) (1.9)	26.22 (0.10)	-2.96 (0.07)	-0.32 (0.11)	0.21	W	N
A7	524	1.00	71.3 (2.9) (1.9)	26.20 (0.10)	-2.95 (0.07)	-0.006 (0.020)	0.21	S	N
A8	519	1.00	70.9 (2.9) (1.9)	26.38 (0.09)	-3.06 (0.06)	-0.006 (0.020)	0.20	S	Y

Fit	$N_{\text{fit}}$	$\hat{\chi}_{\text{WF3}}^2$	$H_0$	R11 Rejection			$\sigma_{\text{int}}$	Priors	
				$p_W$	$b_W$	$Z_w$		$Z_w$	$b_W$
A9	448	0.65	72.3 (2.8) (1.8)	26.30 (0.10)	-3.01 (0.07)	-0.26 (0.10)	0.21	N	N
A10	448	0.65	72.1 (2.8) (1.7)	26.31 (0.10)	-3.01 (0.07)	-0.21 (0.07)	0.21	W	N
A11	448	0.66	71.4 (2.7) (1.7)	26.35 (0.07)	-3.04 (0.07)	-0.006 (0.016)	0.21	S	N
A12	448	0.66	70.7 (2.7) (1.6)	26.45 (0.07)	-3.11 (0.05)	-0.006 (0.016)	0.21	S	Y

Global fits: LMC anchor

Fit	$N_{\text{fit}}$	$\hat{\chi}_{\text{WF3}}^2$	$H_0$	T=2.5 Rejection			$\sigma_{\text{int}}$	Priors	
				$p_W$	$b_W$	$Z_w$		$Z_w$	$b_W$
A13	553	1.00	71.3 (3.6) (2.2)	15.54 (0.08)	-3.11 (0.04)	-0.27 (0.14)	0.31	N	N
A14	552	1.00	72.1 (3.4) (2.1)	15.57 (0.07)	-3.11 (0.04)	-0.20 (0.12)	0.31	W	N
A15	551	1.00	74.2 (2.9) (1.9)	15.65 (0.05)	-3.11 (0.04)	-0.003 (0.020)	0.31	S	N
A16	551	1.00	73.9 (2.9) (1.8)	15.67 (0.05)	-3.13 (0.04)	-0.003 (0.020)	0.31	S	Y

Fit	$N_{\text{fit}}$	$\hat{\chi}_{\text{WF3}}^2$	$H_0$	T=2.25 Rejection			$\sigma_{\text{int}}$	Priors	
				$p_W$	$b_W$	$Z_w$		$Z_w$	$b_W$
A17	523	1.00	69.9 (3.2) (2.0)	15.49 (0.07)	-3.11 (0.04)	-0.38 (0.12)	0.21	N	N
A18	523	1.00	70.5 (3.2) (2.0)	15.52 (0.07)	-3.11 (0.04)	-0.31 (0.11)	0.21	W	N
A19	519	1.00	74.2 (2.8) (1.8)	15.65 (0.05)	-3.11 (0.04)	-0.006 (0.020)	0.20	S	N
A20	518	1.00	73.9 (2.8) (1.7)	15.68 (0.05)	-3.14 (0.04)	-0.006 (0.020)	0.20	S	Y

Fit	$N_{\text{fit}}$	$\hat{\chi}_{\text{WF3}}^2$	$H_0$	R11 Rejection			$\sigma_{\text{int}}$	Priors	
				$p_W$	$b_W$	$Z_w$		$Z_w$	$b_W$
A21	448	0.65	72.1 (3.1) (1.7)	15.58 (0.06)	-3.13 (0.03)	-0.22 (0.10)	0.21	N	N
A22	448	0.65	72.5 (3.0) (1.7)	15.60 (0.06)	-3.13 (0.03)	-0.18 (0.09)	0.21	W	N
A23	448	0.66	74.2 (2.7) (1.7)	15.68 (0.04)	-3.14 (0.03)	-0.005 (0.016)	0.21	S	N
A24	448	0.66	73.9 (2.6) (1.5)	15.70 (0.04)	-3.15 (0.03)	-0.005 (0.016)	0.21	S	Y

Global fits: MW Cepheids anchor

Fit	$N_{\text{fit}}$	$\hat{\chi}_{\text{WF3}}^2$	$H_0$	T=2.5 Rejection			$\sigma_{\text{int}}$	Priors	
				$M_W$	$b_W$	$Z_w$		$Z_w$	$b_W$
A25	552	1.00	82.0 (3.9) (3.6)	-5.85 (0.05)	-2.96 (0.08)	-0.31 (0.13)	0.31	N	N
A26	549	1.00	82.1 (3.9) (3.5)	-5.85 (0.05)	-2.96 (0.08)	-0.20 (0.12)	0.29	W	N
A27	551	1.00	80.2 (3.7) (3.4)	-5.85 (0.05)	-3.00 (0.08)	-0.004 (0.020)	0.31	S	N
A28	551	1.00	77.7 (3.4) (3.0)	-5.87 (0.05)	-3.08 (0.06)	-0.006 (0.020)	0.30	S	Y

Fit	$N_{\text{fit}}$	$\hat{\chi}_{\text{WF3}}^2$	$H_0$	T=2.25 Rejection			$\sigma_{\text{int}}$	Priors	
				$M_W$	$b_W$	$Z_w$		$Z_w$	$b_W$
A29	522	1.00	81.2 (3.6) (3.3)	-5.86 (0.05)	-2.99 (0.06)	-0.45 (0.12)	0.20	N	N
A30	521	1.00	80.9 (3.6) (3.3)	-5.86 (0.05)	-2.99 (0.07)	-0.36 (0.11)	0.20	W	N
A31	514	1.00	81.2 (3.5) (3.2)	-5.85 (0.06)	-2.96 (0.06)	-0.007 (0.020)	0.18	S	N
A32	519	1.00	77.8 (3.3) (2.9)	-5.87 (0.05)	-3.08 (0.05)	-0.006 (0.020)	0.20	S	Y

Fit	$N_{\text{fit}}$	$\hat{\chi}_{\text{WF3}}^2$	$H_0$	R11 Rejection			$\sigma_{\text{int}}$	Priors	
				$M_W$	$b_W$	$Z_w$		$Z_w$	$b_W$
A33	448	0.66	79.9 (3.2) (2.8)	-5.87 (0.04)	-3.05 (0.06)	-0.25 (0.11)	0.21	N	N
A34	448	0.66	79.5 (3.2) (2.8)	-5.87 (0.04)	-3.06 (0.06)	-0.20 (0.10)	0.21	W	N
A35	448	0.67	78.2 (3.1) (2.7)	-5.87 (0.04)	-3.08 (0.06)	-0.006 (0.016)	0.21	S	N
A36	448	0.67	76.6 (2.8) (2.4)	-5.87 (0.04)	-3.14 (0.05)	-0.005 (0.016)	0.21	S	Y

**Table A1.** Fits as in Tables 2 and 3, but using all Cepheids in the R11 sample with periods less than 205 days. The columns are as defined in Table 2.